



# Optimization of a Transcatheter Heart Valve Frame Using Patient-Specific Computer Simulation

GIORGIA ROCATELLO,<sup>1</sup> GIANLUCA DE SANTIS,<sup>2</sup> SANDER DE BOCK,<sup>2</sup> MATTHIEU DE BEULE,<sup>2</sup> PATRICK SEGERS,<sup>1</sup>  
and PETER MORTIER<sup>2</sup>

<sup>1</sup>IBiTech-bioMMeda, Ghent University, Ghent, Belgium; and <sup>2</sup>FEops NV, Technologiepark-Zwijnaarde 122, 9052 Ghent, Belgium

(Received 15 December 2018; accepted 7 June 2019; published online 13 June 2019)

Associate Editor Ajit P. Yoganathan oversaw the review of this article.

## Abstract

**Purpose**—This study proposes a new framework to optimize the design of a transcatheter aortic valve through patient-specific finite element and fluid dynamics simulation.

**Methods**—Two geometrical parameters of the frame, the diameter at ventricular inflow and the height of the first row of cells, were examined using the central composite design. The effect of those parameters on postoperative complications was investigated by response surface methodology, and a Nonlinear Programming by Quadratic Lagrangian algorithm was used in the optimization. Optimal and initial devices were then compared in 12 patients. The comparison was made in terms of device performance [i.e., reduced contact pressure on the atrioventricular conduction system and paravalvular aortic regurgitation (AR)].

**Results**—Results suggest that large diameters and high cells favor higher anchoring of the device within the aortic root reducing the contact pressure and favor a better apposition of the device to the aortic root preventing AR. Compared to the initial device, the optimal device resulted in almost threefold lower predicted contact pressure and limited AR in all patients.

**Conclusions**—In conclusion, patient-specific modelling and simulation could help to evaluate device performance prior to the actual first-in-human clinical study and, combined with device optimization, could help to develop better devices in a shorter period.

**Keywords**—Computer simulation, Design of experiment, Optimization, Patient-specific, Transcatheter aortic valve.

## INTRODUCTION

To date, the design and development phase of new cardiovascular devices is mainly based on benchmark tests and animal experiments, leading to long iterative development cycles. However, in the end, it still remains unclear how the final device will perform in diseased human anatomies, resulting in significant risks for the first patients that undergo treatment with a new device, as well as for the manufacturers of these devices. Using patient-specific computational modelling and simulation during the design and development phase could help to address these challenges.<sup>25</sup> This approach allows to assess the interaction between devices and realistic human anatomies, opening the door towards in-silico clinical trials that could be conducted prior to the actual first-in-human clinical study. In this way, risks for patients and manufacturers can be significantly reduced. In addition, combining patient-specific computational modelling and simulation with device optimization techniques can help to develop better devices in a shorter time period.

Many computational modelling and simulation optimization studies have been performed to find optimal stent geometrical parameters based on mechanical or flow-related objectives: radial strength,<sup>26,27</sup> fatigue resistance,<sup>1,18,19</sup> frame expansion,<sup>18,19</sup> flow disturbances and wall shear stress.<sup>12,23,28</sup> However, the majority of those studies evaluated solely unit stent models,<sup>1</sup> thereby neglecting the interactions with the arterial tissues. Others have used three-dimensional models<sup>12,17,20</sup> and accounted for interactions with simplified vessel geometries.<sup>18,28</sup> Very recently Bosi *et al.*<sup>5</sup> combined patient-specific modeling and optimization techniques to tune the material parameter of the aortic root in 14 patients, to improve

Address correspondence to Peter Mortier, FEops NV, Technologiepark-Zwijnaarde 122, 9052 Ghent, Belgium. Electronic mail: peter.mortier@feops.com

simulation results (i.e., prediction of post-implantation device deformation and paravalvular gaps).

To the best of our knowledge, this is the only available study that combines patient-specific modelling and optimization techniques. However, a device optimization study based on patient-specific modelling has not yet been performed. Such approach could be useful for a wide range of procedures and devices, but this study focuses on transcatheter aortic valve implantation (TAVI).

Clinical studies<sup>9,14,21</sup> have demonstrated the efficacy of TAVI to treat patients with aortic stenosis at extreme- and intermediate-risk. However, complications as paravalvular aortic regurgitation (AR) and conduction abnormalities are considered the Achilles's heel of this treatment. AR has been associated with increased mortality,<sup>7,15,16</sup> whereas conduction abnormalities leading to implantation of permanent pacemaker are associated with increased costs, longer hospital stays and increased patient's morbidity. Considering the prospective of treating younger

patients at low surgical risk, those complications are unacceptable and need to be addressed by improved devices and procedures.

To be effective and prevent migration, TAVI devices need to anchor at or below the annulus of the aortic root. A good apposition between the device and the aortic wall plays a key role in avoiding paravalvular AR. On the other hand, the contact between the stent and the aortic root might generate high pressure on the atrioventricular conduction system which, in turn, might be responsible of conduction abnormalities.

Previous studies have reported that patient-specific computer simulation can be used to predict paravalvular AR and conduction abnormalities after implantation of a CoreValve Revalving System (Medtronic).<sup>4,6,8,22,29</sup>

In this proof-of-concept study, we propose a framework to improve geometric parameters of a representative TAVI device frame through patient-specific computer models able to predict post-operative outcomes.

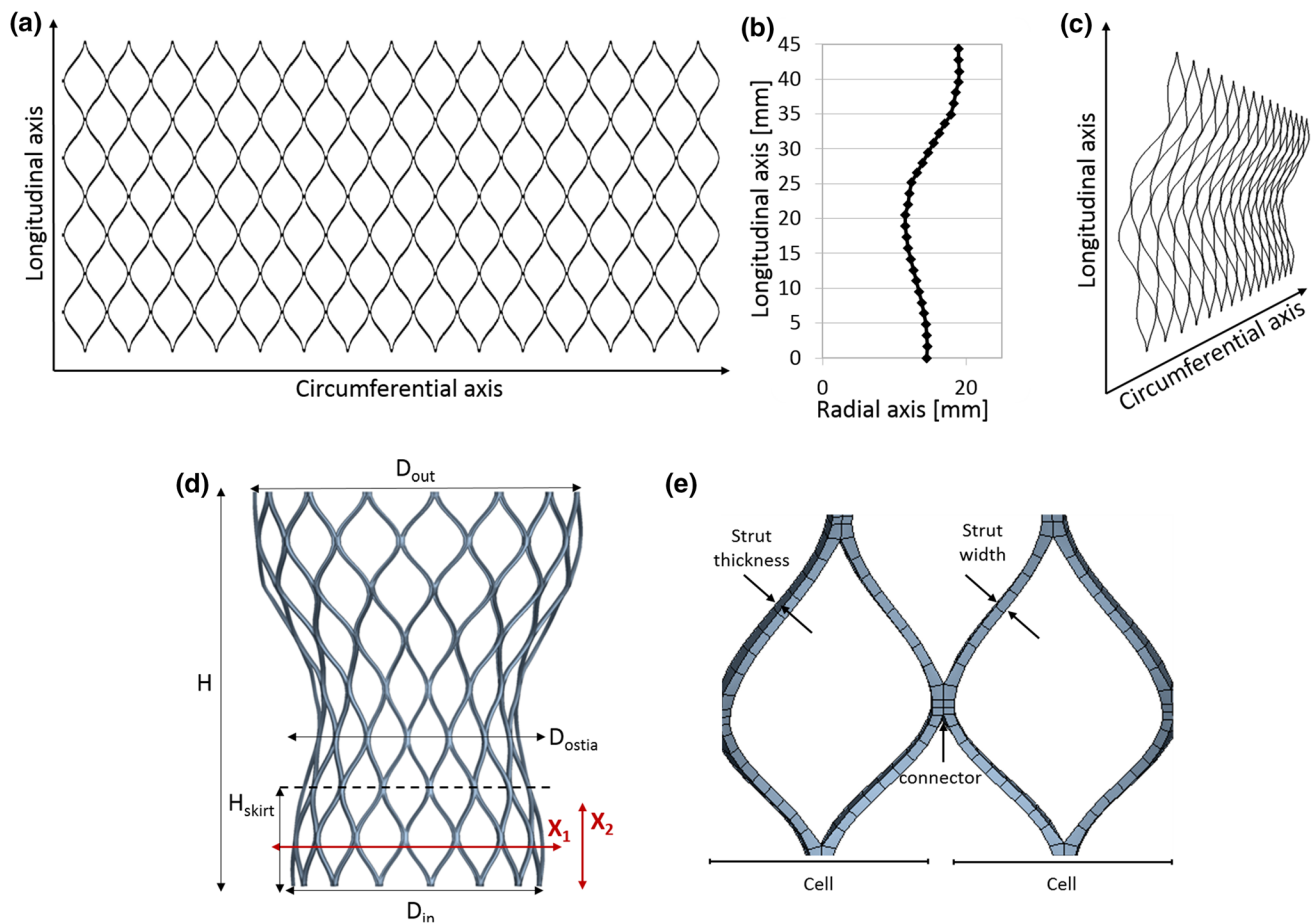


**FIGURE 1.** Valve geometry. (a) unwrapped configuration; (b) profile of the frame of a CoreValve 29 mm; (c) unwrapped configuration with offset; (d) expanded valve configuration, (e) detail of the valve strut. In red the geometrical frame parameters under investigation:  $X_1$  is the diameter at 4 mm above the ventricular inflow,  $X_2$  is the height of the first row of cells.

## MATERIALS AND METHODS

### Valve Geometry and Material Properties

A parametric model of a 29-mm CoreValve-like transcatheter aortic valve was created. The base geometry of the frame was modeled starting from the planar ‘unwrapped’ configuration in pyFormex ([www.nongnu.org/pyformex](http://www.nongnu.org/pyformex)). The ‘unwrapped’ frame design can be seen as a repetition of 15 diamond-like cells along the circumferential axis and 4 diamond-like cells along the longitudinal axis (Fig. 1a). Each cell was described with Cubic Bezier spline interpolation.<sup>11</sup> The profile of the frame of a CoreValve 29 mm (Fig. 1b) was used to generate an offset of the ‘planar’ frame (i.e., varying radius) (Fig. 1c). Finally, the planar frame was ‘wrapped’ to obtain a CoreValve-like shape, in the expanded configuration (Fig. 1d), by applying a coordinate transformation to the nodes of the frame. Geometric parameters of the reference frame design are summarized in Table 1. Briefly, the frame’s height was 46.0 mm, the diameter at the ventricular inflow was 29.0 mm and the diameter at the aortic outflow was 38.0 mm. The strut width and thickness (0.25 mm, 0.45 mm) were in line with literature.<sup>6,13</sup> The frame was modeled with Timoshenko beam elements (B31 in

the Abaqus nomenclature) and WELD connectors were used at the interpolation points between adjacent cells (Fig. 1e). A mesh sensitivity analysis was performed on the device radial force during the crimping and expansion phases. The final stent mesh counted 2670 elements. The material properties of the Nitinol alloy were taken from literature<sup>24</sup> (Table 2).

### Patient-Specific Aortic Root Model

Three-dimensional aortic root models were retrospectively reconstructed from anonymized pre-operative MSCT images of 12 patients, who underwent TAVI in two European centers (Rigshospitalet in Copenhagen, Denmark; Erasmus medical Center in Rotterdam, The Netherlands). Selected patients (3 males, 9 females), between 74 and 89 years old, were considered representative of the TAVI population (e.g., patients with calcified tricuspid or bicuspid aortic valve, heavy calcified valve or sub-annular calcifications). All patients had comparable annular diameters ranging from 23.0 to 26.0 mm. More details of the

**TABLE 1. Frame reference adopted geometrical parameters.**

Parameter	Description	Value (mm)
H	Height	46.0
$D_{in}$	Diameter at ventricular inflow	29.0
$D_{out}$	Diameter at aortic outflow	38.0
$D_{ostia}$	Diameter at ostia level	23.0
$W_{st}$	Strut width	0.25
$th_{st}$	Strut thickness	0.45
$H_{skirt}$	Skirt height	13.0

**TABLE 2. Nitinol material parameters for modeling the frame behavior<sup>24</sup>.**

Parameter	Description	Value
$E^A$	Austenite elastic modulus	51.7 MPa
$E^M$	Martensite elastic modulus	47.8 MPa
$\nu$	Poisson’s ratio	0.3
$\sigma_s$	Start of transformation loading	600 MPa
$\sigma_f$	End of transformation loading	670 MPa
$\sigma_{un}$	Start of transformation unloading	288 MPa
$\sigma_{unf}$	End of transformation unloading	254 MPa
$\epsilon_{Tmax}$	Maximum transformation strain	6.3%
$\epsilon_V$	Maximum volumetric transformation strain	6.3%

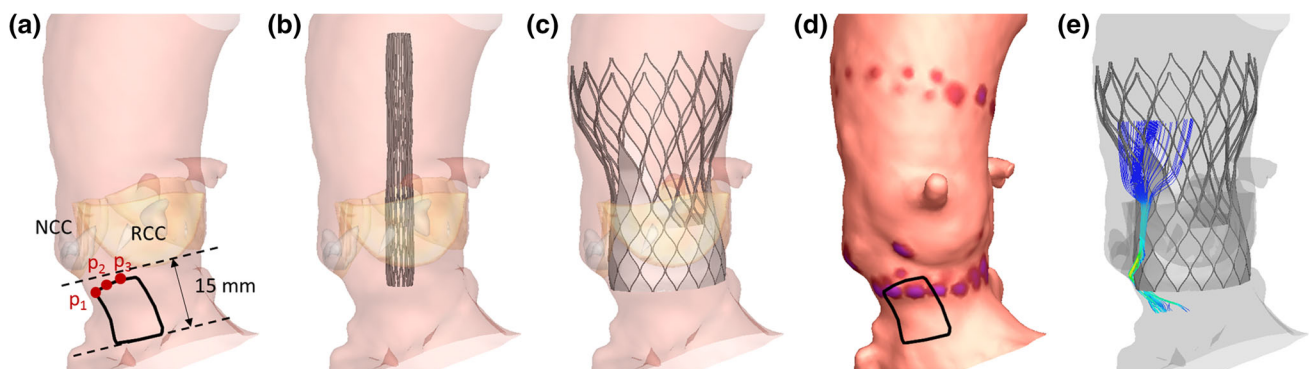


**FIGURE 2. Computer simulation strategy. (a) Patient-specific 3D reconstruction of the aortic root and the region of the atrioventricular conduction system (in red the 3 anatomical landmarks identified using pre-operative CT images); (b) positioning of the crimped device within the aortic root; (c) deployment of the device using FE computer simulation; (d) extraction of contact pressure output within the region of the atrioventricular conduction system; (e) CFD simulation and predicted regurgitant jets. CT = computed tomography. NCC = noncoronary cusp. RCC = right-coronary cusp.**

selected patients are reported in Table 3. Three-dimensional aortic root models consisted of the left-ventricular outflow tract (LVOT), the sinotubular junction and calcified aortic leaflets and ascending aorta (Fig. 2a). Linear elastic models rather than a more realistic but complex hyperelastic anisotropic description were adopted to describe the aortic root tissues. Modelling parameters were derived in a previous study<sup>31</sup> with an iterative process of back-calculations using pre and postoperative MSCT of 39 patients. The aortic wall had an elastic modulus of 2 MPa and a uniform thickness of 2 mm. For the aortic leaflets, elastic modulus of 0.6 MPa and uniform thickness of 1.5 mm was adopted.<sup>3,10</sup> Calcifications were modeled using a stiffer elastic material with perfect plasticity ( $E = 4$  MPa,  $\nu = 0.3$ , yield stress = 0.6 MPa).<sup>29,31</sup> Spring elements were added at each node of the aortic wall to incorporate the impact of surrounding structures in the model.

In each 3D aortic root model, the region of the atrioventricular conduction system was identified as previously described.<sup>29</sup> Briefly, the inferior border of the membranous septum was identified in the pre-operative CT images through three dedicated landmarks (Fig. 2a). Two of these landmarks were selected at the beginning and at the end of the inferior border of the membranous septum, namely  $p_1$  and  $p_3$ , with  $p_1$  closer to the non-coronary cusp (NCC) and  $p_3$  closer to the right coronary cusp (RCC). An additional point ( $p_2$ ) was selected in between to better track the course of the inferior border of the membranous septum as this is often not a straight line. Starting from these anatomical landmarks, the region of the atrioventricular conduction system was defined by the area between the inferior border of the membranous septum (extended towards the RCC by a 25° angle) and the

plane 15 mm below the annulus (Fig. 2a). The model of the patient-specific anatomy was pre-processed using TAVIguide (FEops, Gent, Belgium).

#### Computer Simulation Strategy and Output Variables

Finite-element (FE) simulations were performed using Abaqus/Explicit (v2017, Dassault Systemes Simulia Corp, Johnson, RI). The computer simulation strategy can be subdivided in three steps. In the first step, the device was crimped into the catheter (6 mm diameter), using a cylindrical surface.

In the second step, the device was positioned coaxially within the aortic root (Fig. 2b), and the catheter was retracted leading to the expansion of the device. The default general contact with finite sliding between all the surfaces was used, assuming a coefficient of friction of 0.7 between the valve frame and the aortic model. In all patients, the device was implanted at approximately 4 mm below the aortic annulus (Fig. 2c). In order to evaluate the risk of occurrence of new conduction abnormalities, the maximum contact pressure and the contact pressure index (i.e., the percentage of this region of interest subjected to contact pressure) within the region of the atrioventricular conduction system were extracted (Fig. 2d). The contact pressure index was calculated according to the following formula:

$$\frac{Area_{ROI(\text{where } CP > 0)}}{Area_{ROI}} \times 100, \quad (1)$$

where ROI is the region of interest for the atrioventricular conduction system and CP is the contact pressure.

As third step, a static computational fluid-dynamics (CFD) simulation was performed using the ico-FOAM

TABLE 3. Patients selected for the study.

Patient	Age at TAVI	Gender	Received device (size)	Post-TAVI Paravalvular AR	Post-TAVI Conduction abnormalities
1	79	M	Evolut R (29)	Mild	–
2	89	F	Evolut R (29)	Mild	--
3	76	M	Evolut R (29)	Trace	--
4	86	F	Evolut R (29)	Mild	--
5	78	M	Evolut R (29)	Mild to moderate	--
6	77	F	CoreValve (29)	Mild to moderate	--
7	88	F	CoreValve (29)	Mild to moderate	Total AVB
8	77	F	CoreValve (29)	Trace	LBBB
9	80	F	CoreValve (29)	Mild	LBBB
10	84	F	CoreValve (29)	Trace	LBBB
11	74	F	Lotus (25)	None	–
12	–	F	Lotus (23)	None	–

The ‘received device’ column refers to the device that was implanted in each patient during TAVI. The last two columns report clinical outcomes in form of paravalvular AR and conduction abnormalities.

‘–’ No conduction abnormalities occurred after TAVI. AR = Aortic regurgitation. TAVI = Transcatheter aortic valve implantation.

solver available in OpenFOAM (OpenFOAM, v2.1.1, OpenCFD Ltd., Bracknell, UK). Ico-FOAM is a transient solver for laminar flow. Briefly, the deformed geometries (aortic root and device) were extracted from the FE analysis and a skirt was added to the TAVI device. The fluid domain was extended with cylindrical flow extensions of 8 diameters at the inlet (aortic side) and 3 diameters at the outlet (ventricular side). The extended flow domain was discretized using hexahedral elements and refined within the region of interest (i.e., the lumen within the rigid aortic root wall). The blood was modeled as Newtonian fluid ( $\rho = 1060 \text{ kg/m}^3$ ,  $\mu = 3.5 \times 10^{-3} \text{ Pa s}$ ). No slip condition was described at the aortic wall. A fixed transaortic pressure difference of 32 mmHg was im-

posed to calculate the inlet flow and the location and the velocity of regurgitant jets (Fig. 2e). The imposed pressure difference value is the average of the post-operative end-diastolic transaortic pressure difference retrospectively observed in a sample of 20 patients.<sup>8</sup> This value is in line with the post-operative end-diastolic transaortic pressure difference observed by Sinning *et al.*<sup>32</sup> in a cohort of 146 patients ( $33.8 \pm 12.3 \text{ mmHg}$ ). This analysis was previously validated for prediction of paravalvular AR after implantation of a CoreValve System.<sup>8</sup>

Results from finite-element and fluid-dynamics simulations were post-processed using the TAVIguide software.

**TABLE 4.** Tested levels of experimental variables  $X_1$  and  $X_2$  in the initial design space.

Parameter	Initial coded levels of variables				
	$-\alpha$	$-1$	$0$	$+1$	$+\alpha$
Valve diameter at 4 mm above the ventricular inflow (mm)					
$X_1$	24.9	26.1	29.0	31.9	33.1
Height of the first row of cells at the ventricular inflow (mm)					
$X_2$	5.7	6.4	8.0	9.6	10.3

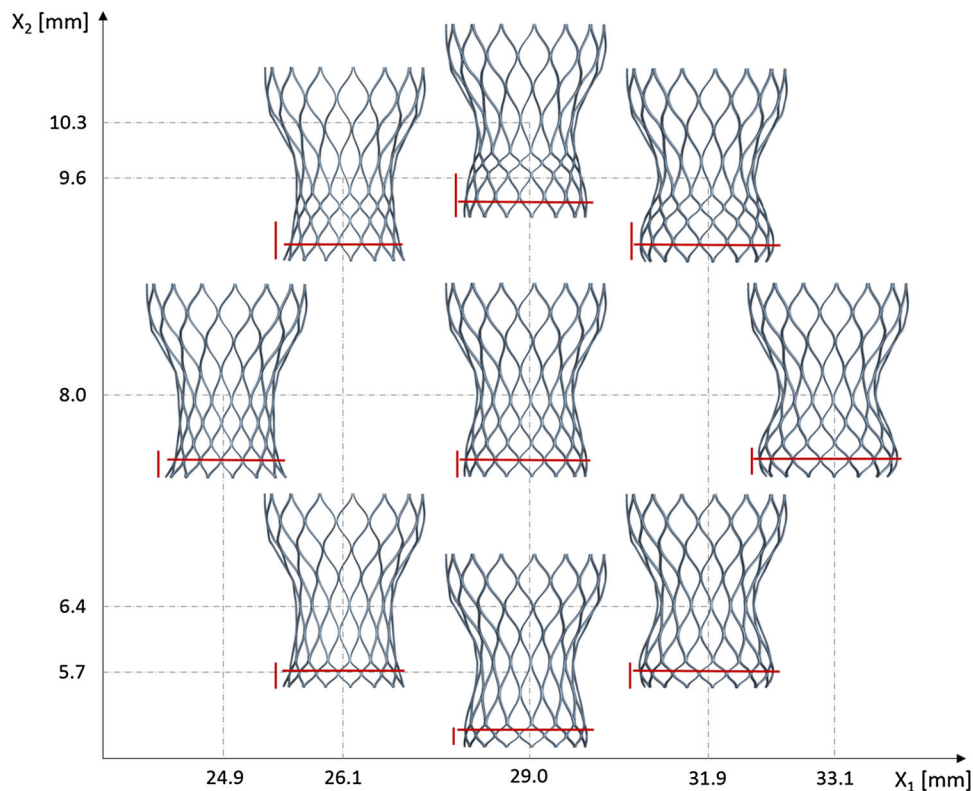


**FIGURE 3.** Frame designs obtained with the experimental variables  $X_1$  and  $X_2$  from the initial design space. Geometrical parameters  $X_1$  and  $X_2$  are represented in red.

### Experimental Design

The central composite design (CCD) was applied to determine the best combination of the frame parameters to reduce conduction abnormalities and paravalvular AR after TAVI. Given the fact that the inflow portion of the device frame plays a crucial role in the anchoring and apposition to the aortic root as well as in the above-mentioned clinical outcomes, we selected two geometrical parameters in this region of the frame. These two parameters are: the valve diameter at 4 mm above the ventricular inflow ( $X_1$ , mm) and the height of the first row of cells at the ventricular inflow ( $X_2$ , mm) (Fig. 1b). Initial value for  $X_1$  is 29.0 mm and for  $X_2$  is 8.0 mm. The initial design space was limited by  $X_1 \pm 10\%$  and  $X_2 \pm 20\%$ . The parameter levels are coded as  $-\alpha$  (low axial level),  $-1$  (low level),  $0$  (central point),  $+1$  (high level) and  $+\alpha$  (high axial level), with  $\alpha$  equals  $\sqrt{2}$ . Independent variables and their levels for the CCD used in the initial design space are shown in Table 4. The designs of the frame obtained with the different combination of the geometrical parameters ( $X_1$  and  $X_2$ ) based on the initial design space are shown in Fig. 3. A qualitative analysis of the effects of the two parameters on the outputs showed that high  $X_1$  and  $X_2$  parameters were associated with low values of the outputs. Detailed results obtained from the analysis in the initial design space can be found in Online Appendix 1. Based on the effects of the two selected geometrical frame parameters on the outputs, subsequent refinement of the design space was performed. Independent variables and their levels for the CCD used in the refined design space are shown in Table 5.

### Response Surface Methodology

A second-order polynomial response surface model (RSM) was used to fit the predicted outputs that are the maximum contact pressure and the contact pressure index (FE outputs) and the paravalvular AR (CFD output). As the study aim was to minimize the outputs predicted from the implantation of each device in all patients, their value averaged over all patients

was considered. The fitting was based on the minimization of the residual error measured by sum of squared deviations between the actual and the estimated response. The second-order polynomial equation has been assumed as:

$$Y = B_0 + \sum_{i=1}^2 B_i X_i + \sum_{i=1}^2 B_{ii} X_i^2 + \sum_{i < j}^2 B_{ij} X_i X_j \pm \varepsilon_r \quad (2)$$

with  $Y$  the value of one output parameter averaged over the 12 patients,  $B$  the coefficients,  $X$  the experimental variables and  $\varepsilon_r$  the error associated with the model. Only the most significant terms from the polynomial equation were selected using the Exhaustive Search method.

The quality of the model was assessed by coefficients of determination:  $R^2$ , *adjusted*  $R^2$ , *predicted*  $R^2$ , and residuals.  $R^2$  represents a pure correlation between measured and predicted values and is indicative of the response variation explained by the model. *Adjusted*  $R^2$  is used to compare the explanatory power of the model, and its value increases only if an added term improves the model. The *predicted*  $R^2$  assesses the predictive power of the model for new observations. This coefficient was calculated by systematically removing each observation from the data set, estimating the regression equation and determining how well the model predicted the removed observation.<sup>2</sup> Residual plots present the difference between the actual and the predicted values and were used to assess whether the coefficients predictions were biased. All analyses were performed in Isight (Dassault Systemes Simulia Corp, Johnson, RI).

### Optimization Strategy

The Nonlinear Programming by Quadratic Lagrangian (NLPQL) was adopted as optimization algorithm, under the assumption that the objective functions are continuously differentiable.<sup>30</sup> The three objective functions were rescaled to have a value between 0 and 1 (Eq. (3)) and combined into a single-objective function using a weighted sum method (Eq. (4)):

TABLE 5. Tested levels of experimental variables  $X_1$  and  $X_2$  in the refined design space.

Parameter	Initial coded levels of variables				
	$-\alpha$	$-1$	$0$	$+1$	$+\alpha$
Valve diameter at 4 mm above the ventricular inflow (mm)					
$X_1$	28.4	29.0	30.5	31.9	32.5
Height of the first row of cells at the ventricular inflow (mm)					
$X_2$	7.7	8.0	8.8	9.6	9.9

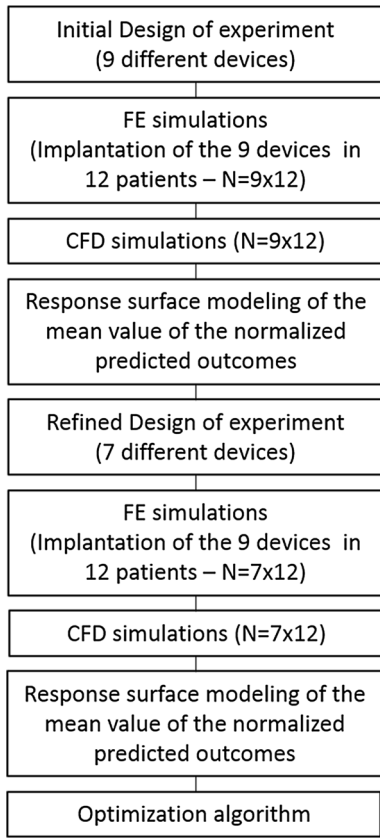


FIGURE 4. Pipeline that has been followed in this study.

$$y_i = \frac{x_i}{\max(x)} \quad (3)$$

$$\sum_{i=1}^3 w_i O_i(X_1, X_2) \quad (4)$$

In Eq. (3)  $x_i$  is a value of one output and  $y_i$  is the corresponding rescaled value.

In Eq. (4),  $w_i$  is the weight of each objective and  $O_i$  are the objectives (RSM functions). In this study, the single-objective function built to minimize the maximum contact pressure ( $O_1$ ), the contact pressure index ( $O_2$ ) and the paravalvular AR ( $O_3$ ) was:

$$0.5O_1(X_1, X_2) + 0.5O_2(X_1, X_2) + 1.0O_3(X_1, X_2) \quad (5)$$

The weight factors accounted for the fact that maximum contact pressure ( $O_1$ ) and contact pressure index ( $O_2$ ) are both predictors of new conduction abnormalities.

Lastly, the performance of the device with the optimal parameters was compared with the performance of the initial device in each patient. The one-tailed Wilcoxon rank test in SPSS (version 22.0, IBM Corporation, New York) was performed to verify whether the improvement in the predicted outcomes

TABLE 6. Quality of the RSM models.

RSM models	$R^2$	Adjusted $R^2$	Predicted $R^2$
$O_1$	0.92	0.89	0.81
$O_2$	0.94	0.93	0.86
$O_3$	0.89	0.86	0.74

was statistically significant. The predicted maximum contact pressure, contact pressure index and paravalvular AR are reported as mean (standard deviation).

Figure 4 summarizes the workflow of the method used in this study.

## RESULTS

In total, 16 devices were created in this study: 9 devices based on the initial design space and 7 additional ones based on the refined design space. Each device was implanted in 12 patients (FE simulation) and, subsequently, a CFD simulation was performed for each patient to derive the paravalvular AR (Fig. 4). Therefore, this study counted 192 FE simulations and same amount of CFD simulations.

Average time for FE simulation was 53 min on a cluster with 16 computing cores (@ 4.0 GHz and 63.0 GB RAM for each node). All CFD simulations were performed on 2 cores (@ 3.2 GHz and 15.2 GB RAM for each node). Average time was 3 h and 50 min.

### Goodness of Fit

The CCD was used to provide good fitting with a second-order polynomial function. RSM polynomial models for maximum contact pressure ( $O_1$ ), contact pressure index ( $O_2$ ) and paravalvular AR ( $O_3$ ) are respectively:

$$O_1 = 3.57 - 0.08X_1 - 0.01X_2^2$$

$$O_2 = 70.38 - 3.92X_2 - 0.02X_1^2$$

$$O_3 = 0.23 + 4.15X_2 - 0.11X_1X_2$$

The coefficient of determination  $R^2$ , adjusted  $R^2$  and predicted  $R^2$  of the models are reported in Table 6.

The coefficient of determination  $R^2$  for all models was higher than 0.89, which indicates a good approximation of the actual function at the design points used for its construction (Fig. 5a). The predicted  $R^2$  [0.74–0.86] was in reasonable agreement with the adjusted  $R^2$

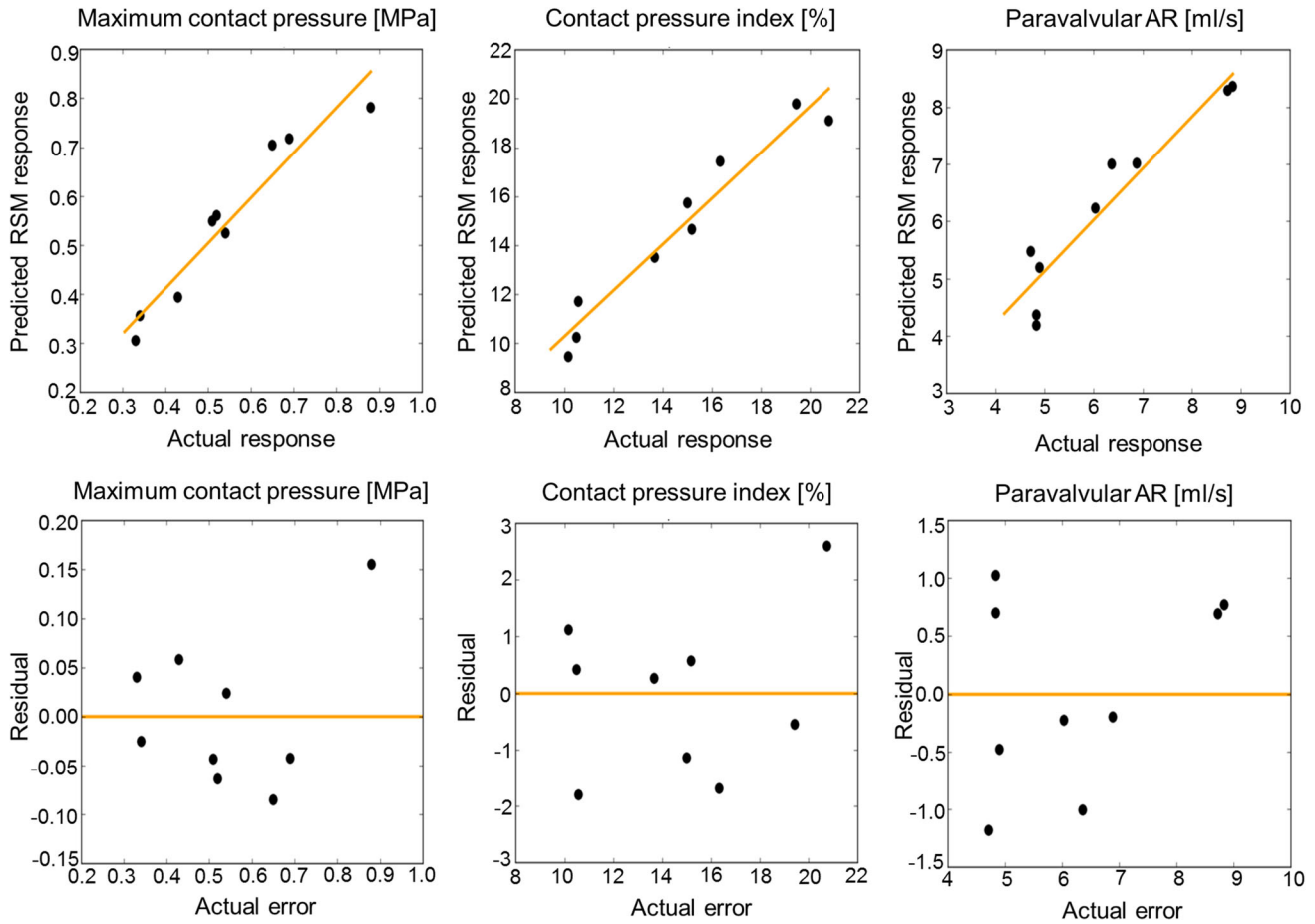


**FIGURE 5.** (a) Plot of the actual and predicted responses and (b) of the actual and residual errors at each design point (black dots). Residuals are defined as the difference between the actual and the predicted responses.

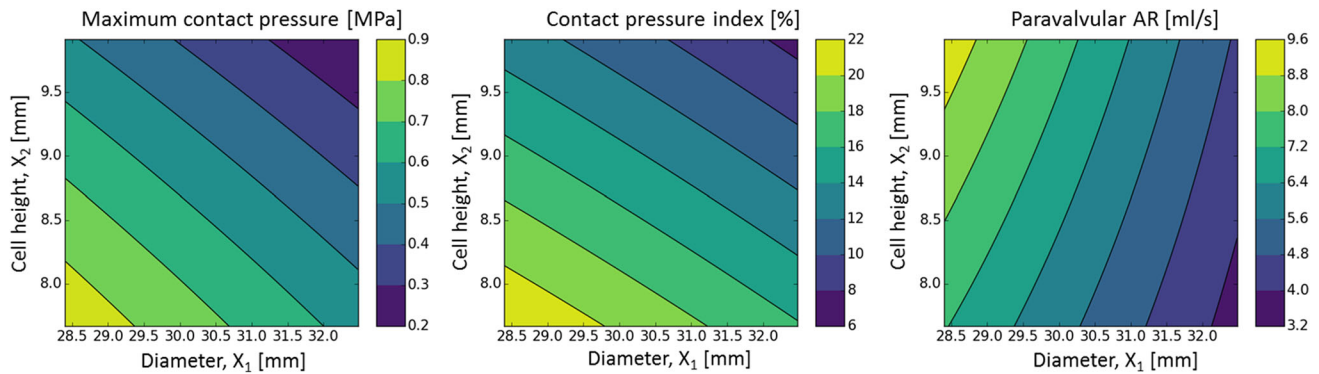


**FIGURE 6.** Contour plot of the response surface models of the maximum contact pressure, contact pressure index and paravalvular AR, respectively from the left to the right. AR = aortic regurgitation.

[0.86–0.93], indicating good predictive power of the model. Residual plots (Fig. 5b) indicated that the coefficients prediction was not biased.

The models have high  $R^2$ ,  $adjusted\ R^2$ ,  $predicted\ R^2$  and random distribution of residual errors. These

results indicate a good fit of the experimental data and high precision in predicting maximum contact pressure, contact pressure index and paravalvular AR. Therefore, the polynomial models were used for further analysis.



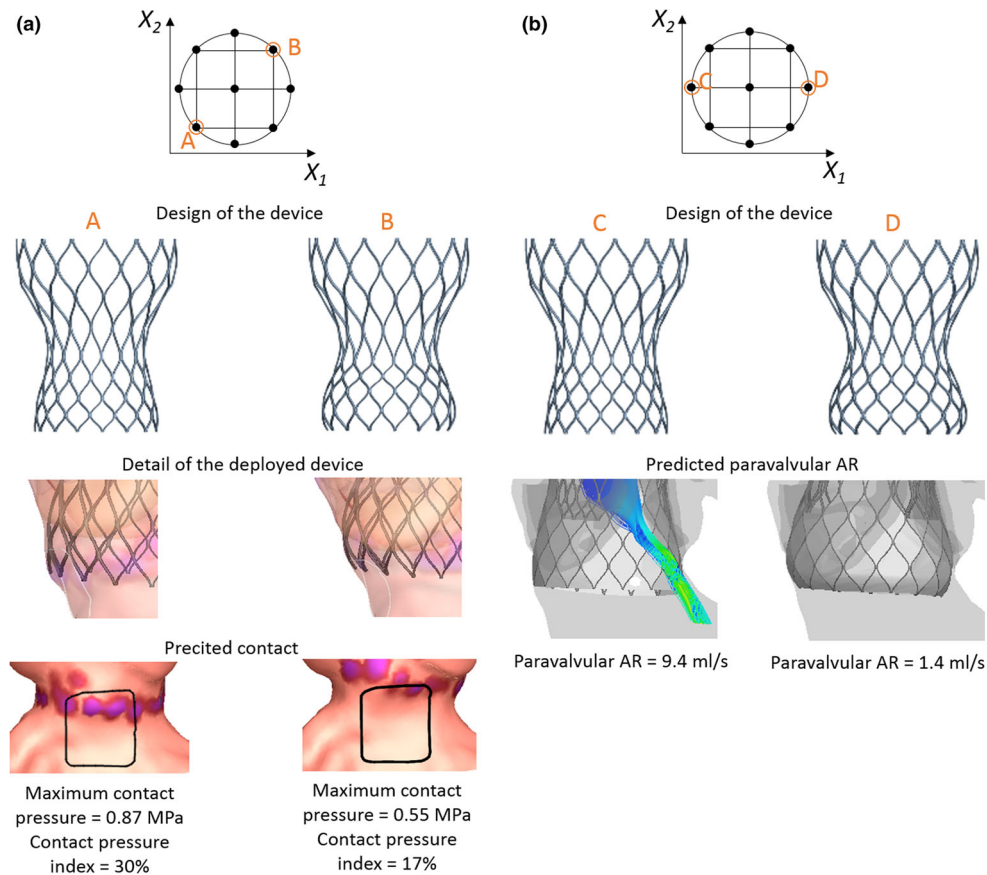


**FIGURE 7.** Representative examples of the effect of the geometrical parameters on maximum contact pressure and contact pressure index (a), and paravalvular AR (b). At the top, a schematic representation of the CCD. (a) A device with low  $X_1$  and low  $X_2$  (A) results in high maximum contact pressure and contact pressure index. Whereas, a device with high  $X_1$  and high  $X_2$  (B) results in low contact within the region of the atrioventricular conduction system. (b) A device with low  $X_1$  (C) results in high paravalvular AR, whereas high  $X_1$  (D) prevents paravalvular AR. AR = aortic regurgitation. CCD = central composite design.

#### *Effects of the Geometrical Parameters*

Two-dimensional contour plots of the RSM models are shown in Fig. 6. High values of maximum contact pressure were observed for low  $X_1$  and  $X_2$ . The diameter at the ventricular inflow of the device ( $X_1$ ) influences its profile. Small diameters determine a sharp profile of the frame, while large diameters make the profile rounder (Fig. 7a). Therefore, small diameters are associated with local spots of contact with high maximum contact pressure. In addition, short cells ( $X_2$ ) at the ventricular inflow of the frame increase the radial force, contributing to high maximum contact pressure on the aortic wall at the region of the ventricular inflow of the device.

The RSM model of the contact pressure index showed a comparable behavior as for the maximum contact pressure. High values of contact pressure index were observed for low  $X_1$  and  $X_2$ . The diameter ( $X_1$ ) and, therefore, the profile of the frame, strongly influences the level at which the device anchors to the aortic annular region. Large diameters (round profile)

favor a higher anchoring level compared to small diameters (sharp profile). As the contact pressure index is a measure of the area of contact between the device and the aortic wall within the region of the atrioventricular conduction system, large diameters (high anchoring level) reduce the area of contact and are associated with low values of contact pressure index. On the contrary, the devices with small diameter (sharp profile) often anchor at the level of the atrioventricular conduction system, resulting in high contact pressure index value (Fig. 7a). Also, short cells ( $X_2$ ), associated with higher radial force, favor the expansion of the frame, contributing to an increase in contact and, hence, the contact pressure index.

With respect to the paravalvular AR, large diameters ( $X_1$ ) and short cells ( $X_2$ ) favor a better apposition of the device to the aortic root, reducing paravalvular AR (Fig. 7b). However, the diameter seems to have a larger influence on the output compared to the height of the cells.

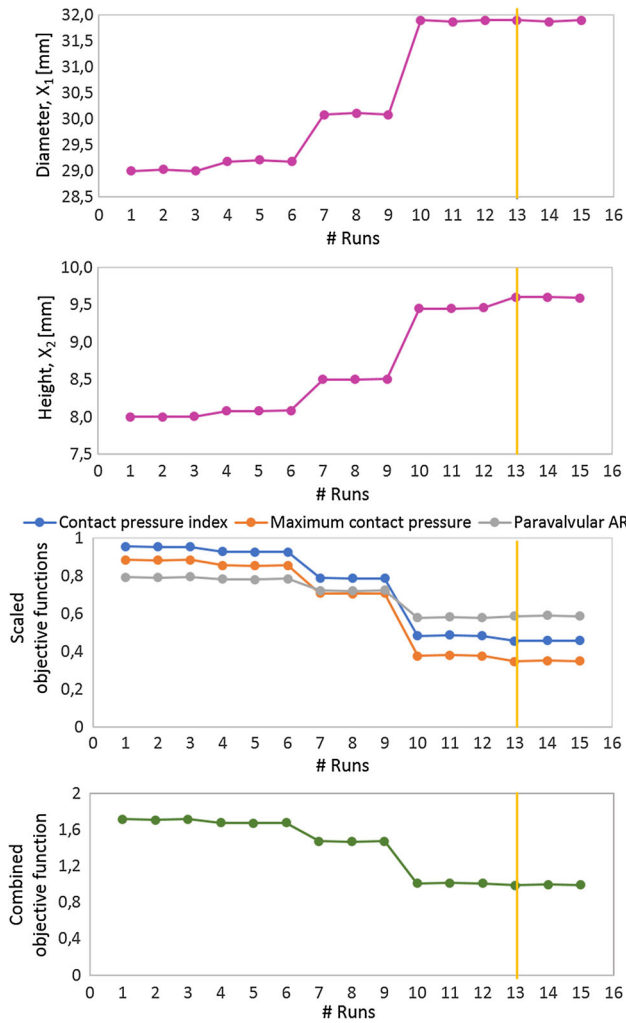


**FIGURE 8. Optimization history of the objectives-function. The location of the minimum is indicated by the orange line.**

*Optimization Results*

Figure 8 reports the optimization history with NLPQL algorithm for the three objectives  $O_1$ ,  $O_2$ ,  $O_3$ . The orange line indicates the position where the minimum is located (# Run 13). The starting point corresponds to the initial design parameters:  $X_1 = 29.0$  mm and  $X_2 = 8.0$  mm. The optimal parameters are:  $X_1 = 31.9$  mm and  $X_2 = 9.6$  mm. The optimized device is shown in Fig. 9.

Figure 10 reports the maximum contact pressure, contact pressure index and paravalvular AR obtained in each patient after implantation of the device with the initial and the optimized design.

The optimized device was associated with lower maximum contact pressure and contact pressure index in all patients. The mean value of maximum contact pressure associated with the optimized device was almost threefold lower compared to the initial device (0.33 vs. 0.88 MPa). Similarly, the mean value of

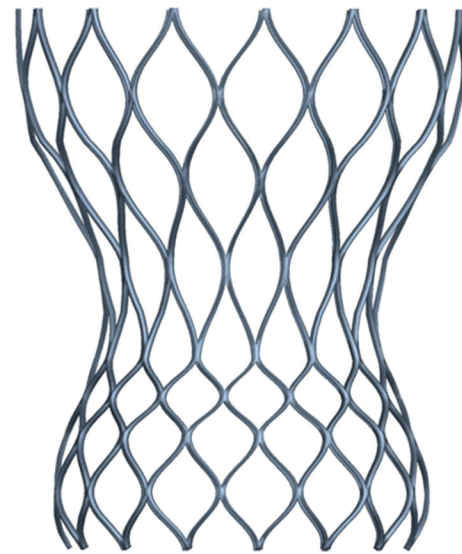


**FIGURE 9. Optimal frame design.**

contact pressure index was twofold lower (10% vs. 19%). The standard deviation slightly decreased as well with the optimized device. With regard to paravalvular AR, the average value decreased from 6.9 to 4.9 ml/s with the optimized device. Although in some patients paravalvular AR slightly increased with the optimized device, the Wilcoxon rank test confirmed that improvement in maximum contact pressure, contact pressure index as well as paravalvular AR is statistically significant ( $p$  value was found  $\leq 0.001$  and  $\leq 0.05$  for the contact pressure-related parameters and for AR respectively).

**DISCUSSION**

This proof-of-concept study presents an optimization workflow based on patient-specific computer simulation to improve the TAVI device performance in reducing the predicted paravalvular AR and conduction abnormalities after TAVI. The central composite design along with the NLPQL algorithm were adopted to optimize two geometrical parameters of a CoreValve-like device: the diameter at 4 mm above the ventricular inflow and the height of the first row of cells. The effect of the design parameters on the objectives was studied using RSM. Results suggest that large diameters and high height of the first row of cells favor a better apposition of the device to the aortic wall avoiding paravalvular AR, and lead to an anchoring level above the location of the atrioventricular conduction system preventing conduction abnormalities. The optimized device showed improved performance in all patients. Maximum contact pressure and contact pressure index that are predictive for

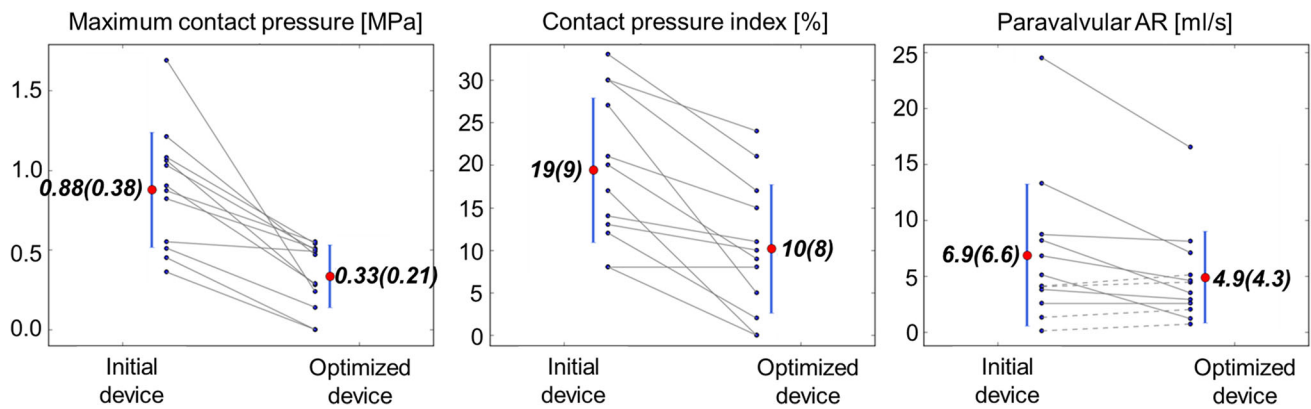


**FIGURE 10.** Comparison of performance between the optimized and initial designs. Continuous grey lines represent a decrease in maximum contact pressure, contact pressure index or paravalvular AR in the same patient. Dotted grey lines represent an increase in maximum contact pressure, contact pressure index or paravalvular AR in the same patient. Mean (standard deviation) are represented by the red dot and the blue bar respectively.

conduction abnormalities lowered with the optimized device. Predicted paravalvular AR was also reduced in 83% of the patients (10/12). Furthermore, good improvement in the design was achieved with only small changes to the geometry which will not change the mechanics or add difficulties in manufacturing.

Most of the existing optimization studies applied to stent geometries, employed computer simulation to improve mechanical properties (stress distribution, radial strength, fatigue resistance) or hemodynamic properties (flow disturbances, wall shear stress). However, optimization was based on mechanical tests performed on solely unit stent models,<sup>1</sup> or simplified 3D stent models<sup>12,17,20</sup> neglecting the interaction with the arterial tissues. Recently, Putra *et al.*<sup>28</sup> adopted computational fluid dynamics simulation to optimize a simplified and idealized two-dimensional stent geometry under the influence of the vessel wall deformation. Li *et al.*<sup>18</sup> accounted for the interaction of the stent with simplified plaque and artery in the optimization of a stent life prediction and stent expansion. Recently, Bosi *et al.*,<sup>5</sup> combined patient-specific modeling with optimization techniques to tune the material parameter of the aortic root in their TAVI simulation workflow.

Though, to the best of our knowledge, this is the first study that adopts full three-dimensional patient-specific models to optimize stent geometrical parameters of a TAVI device, minimizing the predicted clinical complications in the average population. With this approach, the performance of the device can be evaluated in models resembling anatomical variability among patients eligible for TAVI, (aortic root variability, amount and location of calcifications, tricuspid or bicuspid aortic valve) before entering the clinical phase.

This proof-of-concept study shows that computer simulations based on patient-specific anatomies and population-based parameters on a representative

TAVI population can be used to optimize the design of a TAVI device reducing the costs and the time of the design and development phase of a new device, as well as the level of risk during the clinical studies.

This is a valuable approach with the potential to be extended to medical devices in general. The objectives can also be extended to any other clinical outcome as long as computational modelling and simulation can accurately predict those outcomes. In this study, the optimized device is quite similar to the CoreValve system, for which the strategy for predicting paravalvular AR and conduction abnormalities was previously validated.<sup>8,29,31</sup> Due to the similarity between the CoreValve and the device variants modelled in this study, we believe the previous validation work remains valid for these new devices.

While in this study we focused on three key functional post-deployment variables (maximum contact pressure, contact pressure area and paravalvular regurgitation), this approach can be used to optimize any geometrical parameter that plays a relevant role in the performance of the device (i.e., stress distribution, durability of the device). Also, the amount of geometrical parameters under investigation can be increased.

## STUDY LIMITATIONS

Although device optimization based on patient-specific computer simulation has many advantages in the stent design, this study has certain limitations. First, significant computational resources are required to perform this kind of study. A total of 16 devices were created and virtually implanted in 12 patients, resulting in 192 FEA simulations and same amount of CFD simulations. Additionally, iterative repositioning

of the device was necessary in some cases, to reach comparable implantation depth of the device in each patient. In fact, the obtained optimal device is implantation depth-specific. Whether it remains the optimal solution at different implantation depths needs to be verified. Second, a limited number of patients was enrolled in the study. Despite the fact that only 12 patients were used, they were representative of the population eligible for TAVI, and assumed sufficient for a proof-of-concept study. In future, automatization of the entire process is planned, with inclusion of more patients to ensure optimal device performance. Last, this study focused on the prediction of three post-procedural outcomes, but other parameters that play an important role in the performance and durability of the device should be evaluated. For example, the crimping feasibility of those devices should be checked to ensure that the device is not damaged. A mechanical analysis of the stress distribution on the device frame and device leaflets should be performed to guarantee high performance and device durability. Also, mechanical factors that might affect the stress/strain distribution on the aortic wall to avoid negative outcomes (i.e., annulus rupture) should be included in the optimization study.

## CONCLUSION

In this study, we proposed a framework to improve the design of a representative TAVI frame using patient-specific computer models able to predict post-operative outcomes. Results show that this approach can effectively evaluate and optimize the performance of a TAVI device on a virtual TAVI population. The proposed approach can help to speed up the initial design and development phase of new devices and lower the risk during clinical studies.

## ELECTRONIC SUPPLEMENTARY MATERIAL

The online version of this article (<https://doi.org/10.1007/s13239-019-00420-7>) contains supplementary material, which is available to authorized users.

## ACKNOWLEDGMENTS

G. Rocatello is supported by the European Commission within the Horizon 2020 Framework through the Marie Skłodowska-Curie Action-International Training Network (MSCA-ITN) European Training Networks (Project Number 642458). Computer modeling and simulation was performed using the TAVI-guide framework developed at FEops NV.

## CONFLICT OF INTEREST

Matthieu De Beule and Peter Mortier are shareholders of FEops. Sander De Bock and Gianluca de Santis are employees of FEops.

## ETHICAL APPROVAL

For this retrospective study, formal consent is not required. This article does not contain any studies with animals performed by any of the authors.

## INFORMED CONSENT

Informed consent was obtained from all individual participants included in the study.

## REFERENCES

- <sup>1</sup>Alaimo, G., F. Auricchio, M. Conti, and M. Zingales. Multi-objective optimization of nitinol stent design. *Med. Eng. Phys.* 47:13–24, 2017. <https://doi.org/10.1016/j.medengphys.2017.06.026>.
- <sup>2</sup>Allen, D. M. The relationship between variable selection and data augmentation and a method for prediction. *Technometrics* 16(1):125–127, 1974. <https://doi.org/10.2307/1267500>.
- <sup>3</sup>Bailey, J., N. Curzen, and N. W. Bressloff. Assessing the impact of including leaflets in the simulation of TAVI deployment into a patient-specific aortic root. *Comput. Methods Biomech. Biomed. Eng.* 19(7):733–744, 2016. <https://doi.org/10.1080/10255842.2015.1058928>.
- <sup>4</sup>Bianchi, M., G. Marom, R. P. Ghosh, O. M. Rotman, P. Parikh, L. Gruberg, *et al.* Patient-specific simulation of transcatheter aortic valve replacement: impact of deployment options on paravalvular leakage. *Biomech. Model. Mechanobiol.* 2018. <https://doi.org/10.1007/s10237-018-1094-8>.
- <sup>5</sup>Bosi, G. M., C. Capelli, M. H. Cheang, N. Delahunty, M. Mullen, A. M. Taylor, *et al.* Population-specific material properties of the implantation site for transcatheter aortic valve replacement finite element simulations. *J. Biomech.* 71:236–244, 2018. <https://doi.org/10.1016/j.jbiomech.2018.02.017>.
- <sup>6</sup>Bosmans, B., N. Famaey, E. Verhoelst, J. Bosmans, and J. Vander Sloten. A validated methodology for patient specific computational modeling of self-expandable transcatheter aortic valve implantation. *J. Biomech.* 49(13):2824–2830, 2016. <https://doi.org/10.1016/j.jbiomech.2016.06.024>.
- <sup>7</sup>Buzzatti, N., A. Castiglioni, E. Agricola, M. Barletta, S. Stella, F. Giannini, *et al.* Five-year evolution of mild aortic regurgitation following transcatheter aortic valve implantation: early insights from a single-centre experience. *Interact. Cardiovasc. Thorac. Surg.* 25(1):75–82, 2017. <https://doi.org/10.1093/icvts/ivx070>.
- <sup>8</sup>de Jaegere, P., G. De Santis, R. Rodriguez-Olivares, J. Bosmans, N. Bruining, T. Deutzer, *et al.* Patient-specific computer modeling to predict aortic regurgitation after transcatheter aortic valve replacement. *JACC Cardiovasc. Interv.* 9(5):508–512, 2016. <https://doi.org/10.1016/j.jcin.2016.01.003>.

- <sup>9</sup>Deeb, G. M., M. J. Reardon, S. Chetcuti, H. J. Patel, P. M. Grossman, S. J. Yakubov, *et al.* 3-year outcomes in high-risk patients who underwent surgical or transcatheter aortic valve replacement. *J. Am. Coll. Cardiol.* 67(22):2565–2574, 2016. <https://doi.org/10.1016/j.jacc.2016.03.056>.
- <sup>10</sup>Finotello, A., S. Morganti, and F. Auricchio. Finite element analysis of TAVI: impact of native aortic root computational modeling strategies on simulation outcomes. *Med. Eng. Phys.* 47:2–12, 2017. <https://doi.org/10.1016/j.medengphys.2017.06.045>.
- <sup>11</sup>Gessat, M., L. Altwegg, T. Frauenfelder, A. Plass, and V. Falk. Cubic Hermite Bezier spline based reconstruction of implanted aortic valve stents from CT images. *Conf. Proc. IEEE Eng. Med. Biol. Soc.* 2011:2667–2670, 2011. <https://doi.org/10.1109/iembs.2011.6090733>.
- <sup>12</sup>Gundert, T. J., A. L. Marsden, W. Yang, and J. F. LaDisa, Jr. Optimization of cardiovascular stent design using computational fluid dynamics. *J. Biomech. Eng.* 134(1):011002, 2012. <https://doi.org/10.1115/1.4005542>.
- <sup>13</sup>Gunning, P. S., T. J. Vaughan, and L. M. McNamara. Simulation of self expanding transcatheter aortic valve in a realistic aortic root: implications of deployment geometry on leaflet deformation. *Ann. Biomed. Eng.* 42(9):1989–2001, 2014. <https://doi.org/10.1007/s10439-014-1051-3>.
- <sup>14</sup>Kapadia, S. R., M. B. Leon, R. R. Makkar, E. M. Tuzcu, L. G. Svensson, S. Kodali, *et al.* 5-year outcomes of transcatheter aortic valve replacement compared with standard treatment for patients with inoperable aortic stenosis (PARTNER 1): a randomised controlled trial. *Lancet* 385(9986):2485–2491, 2015. [https://doi.org/10.1016/s0140-6736\(15\)60290-2](https://doi.org/10.1016/s0140-6736(15)60290-2).
- <sup>15</sup>Kodali, S., P. Pibarot, P. S. Douglas, M. Williams, K. Xu, V. Thourani, *et al.* Paravalvular regurgitation after transcatheter aortic valve replacement with the Edwards sapien valve in the PARTNER trial: characterizing patients and impact on outcomes. *Eur. Heart J.* 36(7):449–456, 2015. <https://doi.org/10.1093/eurheartj/ehu384>.
- <sup>16</sup>Leon, M. B., C. R. Smith, M. J. Mack, R. R. Makkar, L. G. Svensson, S. K. Kodali, *et al.* Transcatheter or surgical aortic-valve replacement in intermediate-risk patients. *N. Engl. J. Med.* 374(17):1609–1620, 2016. <https://doi.org/10.1056/NEJMoa1514616>.
- <sup>17</sup>Li, H., J. Gu, M. Wang, D. Zhao, Z. Li, A. Qiao, *et al.* Multi-objective optimization of coronary stent using kriging surrogate model. *Biomed. Eng. Online* 15(Suppl 2):148, 2016. <https://doi.org/10.1186/s12938-016-0268-9>.
- <sup>18</sup>Li, H., T. Liu, M. Wang, D. Zhao, A. Qiao, X. Wang, *et al.* Design optimization of stent and its dilatation balloon using kriging surrogate model. *BioMed. Eng. OnLine* 16(1):13, 2017. <https://doi.org/10.1186/s12938-016-0307-6>.
- <sup>19</sup>Li, H., T. Qiu, B. Zhu, J. Wu, and X. Wang. Design optimization of coronary stent based on finite element models. *Sci. World J.* 2013:630243, 2013. <https://doi.org/10.1155/2013/630243>.
- <sup>20</sup>Li, N., H. Zhang, and H. Ouyang. Shape optimization of coronary artery stent based on a parametric model. *Finite Elem. Anal. Des.* 45(6–7):468–475, 2009. <https://doi.org/10.1016/j.finel.2009.01.001>.
- <sup>21</sup>Mack, M. J., M. B. Leon, C. R. Smith, D. C. Miller, J. W. Moses, E. M. Tuzcu, *et al.* 5-year outcomes of transcatheter aortic valve replacement or surgical aortic valve replacement for high surgical risk patients with aortic stenosis (PARTNER 1): a randomised controlled trial. *Lancet* 385(9986):2477–2484, 2015. [https://doi.org/10.1016/S0140-6736\(15\)60308-7](https://doi.org/10.1016/S0140-6736(15)60308-7).
- <sup>22</sup>Mao, W., Q. Wang, S. Kodali, and W. Sun. Numerical parametric study of paravalvular leak following a transcatheter aortic valve deployment into a patient-specific aortic root. *J. Biomech. Eng.* 2018. <https://doi.org/10.1115/1.4040457>.
- <sup>23</sup>Migliavacca, F., L. Petrini, V. Montanari, I. Quagliana, F. Auricchio, and G. Dubini. A predictive study of the mechanical behaviour of coronary stents by computer modelling. *Med. Eng. Phys.* 27(1):13–18, 2005. <https://doi.org/10.1016/j.medengphys.2004.08.012>.
- <sup>24</sup>Morganti, S., N. Brambilla, A. S. Petronio, A. Reali, F. Bedogni, and F. Auricchio. Prediction of patient-specific post-operative outcomes of TAVI procedure: the impact of the positioning strategy on valve performance. *J. Biomech.* 49(12):2513–2519, 2016. <https://doi.org/10.1016/j.jbiomech.2015.10.048>.
- <sup>25</sup>Morrison, T. M., M. L. Dreher, S. Nagaraja, L. M. Angelone, and W. Kainz. The role of computational modeling and simulation in the total product life cycle of peripheral vascular devices. *J. Med. Devices* 11(2):024503, 2017. <https://doi.org/10.1115/1.4035866>.
- <sup>26</sup>Pant, S., N. W. Bressloff, and G. Limbert. Geometry parameterization and multidisciplinary constrained optimization of coronary stents. *Biomech. Model. Mechanobiol.* 11(1–2):61–82, 2012. <https://doi.org/10.1007/s10237-011-0293-3>.
- <sup>27</sup>Pant, S., G. Limbert, N. P. Curzen, and N. W. Bressloff. Multiobjective design optimisation of coronary stents. *Biomaterials* 32(31):7755–7773, 2011. <https://doi.org/10.1016/j.biomaterials.2011.07.059>.
- <sup>28</sup>Putra, N. K., P. S. Palar, H. Anzai, K. Shimoyama, and M. Ohta. Multiobjective design optimization of stent geometry with wall deformation for triangular and rectangular struts. *Med. Biol. Eng. Comput.* 57(1):15–26, 2018. <https://doi.org/10.1007/s11517-018-1864-6>.
- <sup>29</sup>Rocatello, G., N. El Faquir, G. De Santis, F. Iannaccone, J. Bosmans, O. De Backer, *et al.* Patient-specific computer simulation to elucidate the role of contact pressure in the development of new conduction abnormalities after catheter-based implantation of a self-expanding aortic valve. *Circ. Cardiovasc. Interv.* 11(2):e005344, 2018. <https://doi.org/10.1161/circinterventions.117.005344>.
- <sup>30</sup>Schittkowski, K. NLPQL: a fortran subroutine solving constrained nonlinear programming problems. *Ann. Oper. Res.* 5(2):485–500, 1986. <https://doi.org/10.1007/BF02022087>.
- <sup>31</sup>Schultz, C. J., R. Rodriguez-Olivares, J. Bosmans, T. Lefèvre, G. De Santis, N. Bruining, *et al.* Patient-specific image-based computer simulation for the prediction of valve morphology and calcium displacement after TAVI with the Medtronic CoreValve and the Edwards SAPIEN valve. *EuroIntervention* 11(9):1044–1052, 2016. <https://doi.org/10.4244/EIJV11I9A212>.
- <sup>32</sup>Sinning, J. M., A. Stundl, S. Pingel, M. Weber, A. Sedaghat, C. Hammerstingl, *et al.* Pre-procedural hemodynamic status improves the discriminatory value of the aortic regurgitation index in patients undergoing transcatheter aortic valve replacement. *JACC Cardiovasc. Interv.* 9(7):700–711, 2016. <https://doi.org/10.1016/j.jcin.2015.12.271>.

**Publisher's Note** Springer Nature remains neutral with regard to jurisdictional claims in published maps and institutional affiliations.